Design of spatio-temporally modulated static infrared imaging Fourier transform spectrometer

WenCong Wang,[1,2] JingQiu Liang,[1,*] ZhongZhu Liang,[1,3] JinGuang Lü,[1] YuXin Qin,[1] Chao Tian,[1,2] and WeiBiao Wang[1]

[1]*State Key Laboratory of Applied Optics, Changchun Institute of Optics, Fine Mechanics and Physics, Chinese Academy of Sciences, Changchun, Jilin 130033, China*

[2]*University of Chinese Academy of Sciences, Beijing 100049, China*

[3]*e-mail: liangzz@ciomp.ac.cn*

**Corresponding author: liangjq@ciomp.ac.cn*

Received June 2, 2014; revised July 6, 2014; accepted July 6, 2014; posted July 9, 2014 (Doc. ID 213265); published August 14, 2014

A novel static medium wave infrared (MWIR) imaging Fourier transform spectrometer (IFTS) is conceptually proposed and experimentally demonstrated. In this system, the moving mirror in traditional temporally modulated IFTS is replaced by multi-step micro-mirrors to realize the static design. Compared with the traditional spatially modulated IFTS, they have no slit system and are superior with larger luminous flux and higher energy efficiency. The use of the multi-step micro-mirrors can also make the system compact and light. © 2014 Optical Society of America

OCIS codes: (110.3175) Interferometric imaging; (110.3080) Infrared imaging; (070.4790) Spectrum analysis; (120.4570) Optical design of instruments.

http://dx.doi.org/10.1364/OL.39.004911

The imaging Fourier transform spectrometer (IFTS) can acquire three-dimensional information for a target object, i.e., simultaneously obtains two dimensions of image information and one dimension of spectral information. The information can be widely applied in various areas, such as target detection, geological exploration, and environmental monitoring. [1–4].

According to the different ways of producing optical path differences (OPDs) for Fourier transform imaging spectrometer, it can be classified as temporally modulated, spatially modulated, and spatio-temporally modulated [5,6]. Generally speaking, a temporally modulated IFTS has a higher spectral resolution [7,8], but cannot achieve static and compact set-up because of the existence of the moving mirror. A spatially modulated IFTS uses a slit to control the spatial resolution, and can have compact and stable structure [9]. However, its luminous flux is limited by the slit and the system has a relative low usage of the input optical energy. The spatio-temporally modulated IFTS is based on the windowing-interference imaging principle [10]. It has neither a slit nor a moving mirror, and thus offers a large luminous flux as well as a static structure [6,10].

The medium wave infrared (MWIR) is an important spectral band. Many toxic and harmful gases have a strong MWIR absorption band. For example, CO_2 places in 4.3 μm, CO places in 4.8 μm, and SO_2 has a strong absorption peak in 4 μm [11]. Moreover, the aerospace vehicle exhausts and the high-temperature sewage outfall of companies can radiate strongly at MWIR band [12]. In the daytime, the temperature of an aerial target, which mainly radiates a long wave infrared (LWIR) at room temperature, could reach more than 500 K and the peak wavelength of the radiated infrared moves to the MWIR band through absorbing the heat of solar radiation, so the radiation in MWIR band is much stronger than in LWIR band. At night the temperature of the aerial target is around 400 K. The target has the same radiation intensity in MWIR band and LWIR band. However, at this time the radiation of the sky atmospheric background mainly concentrates in the LWIR band. Therefore, the MWIR is the better waveband for detection of the aerial target in these situations with complex background [13]. Above all, the MWIR imaging spectrometer can be widely applied in detection of toxic gases, monitoring of greenhouse, target detection, surface features recognition, pollutant monitoring, aerospace remote sensing etc., [11–14].

In view of the advantages of a spatio-temporally modulated IFTS and the features of the MWIR emissions, this Letter proposes a novel static MWIR spatio-temporally modulated IFTS. The modulation is achieved by a multi-step micro-mirror process. The system has no slit and can have larger luminous flux and higher energy efficiency.

The multi-step micro-mirrors were firstly proposed by Möller to use in static Fourier transform spectrometer and developed by Ivanov and co-workers [15–17]. But the Fourier transform spectrometer could only get the spectral information. As our knowledge, this is the first time to use the multi-step micro-mirror in IFTS.

The layout of the proposed IFTS is shown in Fig. 1. It consists of the scanning mirror, the first imaging system, the beam splitter system, the plane mirror, the multi-step micro-mirrors, the second imaging system and the MWIR

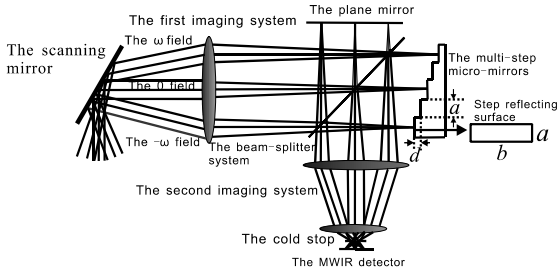

Fig. 1. Layout of the novel IFTS structure.

 © 2014 Optical Society of America

detector. For the multi-step micro-mirrors, the step reflecting surface width is a, the length is b and the step height is d. The plane mirror and one step reflecting surface of the multi-step micro-mirrors are located in the focal plane of the front imaging system. The rest of the step reflecting surfaces of the multi-step micro-mirrors are located in the focal depth of the first imaging system. Thus, the target could be fairly imaged on all the mirrors. The focal depth of the first imaging system can be shown in Eq. (1):

$$\delta_{\text{defocus}} = \frac{\lambda}{2(\text{NA})^2}. \tag{1}$$

In Eq. (1), λ is a working wavelength of the IFTS and the NA is the imaging aperture of the first imaging system. In the first imaging system, the focal depth should be no less than the total step height nd of the multi-step micro-mirrors. Thus, in the process of designing the first imaging system, its NA should meet the requirement that is shown in Eq. (2):

$$\text{NA} \le \sqrt{\frac{\lambda}{2\text{nd}}}. \tag{2}$$

The MWIR detector is located in the image surface of the second imaging system to capture the interferogram generated by the two mirrors.

This system can be used as the payload for the space shuttle or the satellite. Through the motion of the shuttle or the satellite, the image of the target will move in the opposite direction on the multi-level micro-mirror and the detector. Thus, the target image moves at different steps and the windowing process of the system could be achieved. In this manner, we could complete the sample of the interferogram with a different order. In this system, we use a scanning mirror to simulate the windowing process. The working principle is as follows: The light emitted from the target enters the first imaging system with a field angle ω. Then it is imaged by the first imaging system both on the plane mirror and a step reflecting surface of the multi-step micro-mirrors. Because of the height of each step, the two first imaging points that are imaged respectively on the plan mirror and the multi-step micro-mirrors have invariable phase difference. The two imaged points serve as two coherent sources and generate the corresponding interferogram on the MWIR detector, after being re-imaged via the second imaging system. Thus, the image of the target and the interference information with OPD defined by the two mirrors are obtained simultaneously. By the rotation of the scanning mirror, light from the same target but with a different field angle will enter the system and be imaged on an adjacent step reflecting surface by the first imaging system at the next moment. During a completed scanning process, the target will be imaged on all of the step reflecting surfaces and will generate interferograms of different OPDs. Then spectral information can be obtained via a Fourier transform [18,19].

There are several designs of spatio-temporally modulated imaging spectrometers. The imaging spectrometer based on the Michelson with a tilted mirror was demonstrated by Hirai *et al.* [20]. It has a large luminous flux. However, the tilted angle of the mirror is restricted to a small range which results in a relatively low spectral resolution. The imaging system based on the sagnac interferometer static structure has a stable structure, but it has a strict sensitivity to the misalignment of the system [21]. The system with a birefringent interferometer has a stable structure and a large luminous flux, but for the reason of materials of the birefringent crystal prism, it is somewhat difficult to use in MWIR band [7]. Compared to these imaging spectrometers, the IFTS proposed in this Letter has a stable and static structure, as well as a large luminous flux. The spectral resolution could be improved by adding additional steps to the multi-step micro-mirrors.

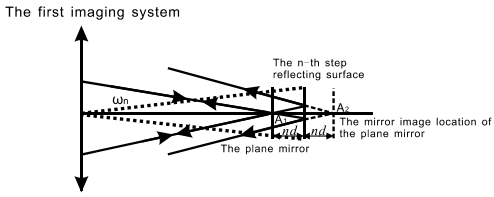

Fig. 2. OPDs produced by the system.

The OPD is introduced by the two mirrors. Figure 2 shows the first imaging process. A_1 is the image of the target that images on the plane mirror. A_2 is a virtual image on a parallel plane to the plane mirror that corresponds to the images on the step mirror, which is introduced to benefit analysis. A_1 and A_2 are two coherent points and could interfere with each other on the MWIR detector. For the height of step d and step number n, the OPD between A_1 and A_2 is

$$\delta = 2\text{nd}. \tag{3}$$

To ensure the invariant of the OPD, the first imaging system utilizes the imaging telecentric structure, thus light within ω_n. has the same OPD.

Figure 3 shows the process of A_1 and A_2 interfering on the MWIR detector. A_1' and A_2' are the images of A_1 and A_2 via the second imaging system. The MWIR detector is located in the midpoint of the A_1' and A_2', where the Airy disk formed by the A_1' and A_2' coincides and interferes in a pixel-size area [22].

As described above, different step reflecting surfaces have different OPDs and correspond to different field angles. As shown in Fig. 4, one step reflecting surface corresponds to two field angles. One is the sagittal field angle W that corresponds to the length b of the step; the other is the meridian field angle ω_n that corresponds to the width a of the step reflecting surface. The sagittal field angle W for a step reflecting surface is:

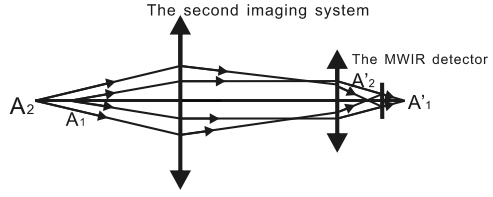

Fig. 3. Interference process on the MWIR detector.

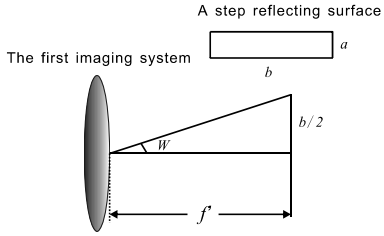

Fig. 4. Schematic diagram of the sagittal field angle corresponding to a step of the reflecting surface.

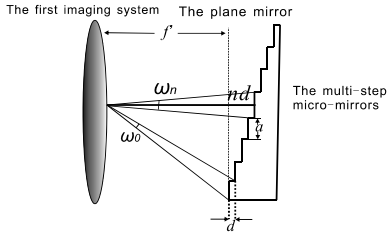

Fig. 5. Schematic diagram of the meridian field angle for one step of the reflecting surface.

$$W = \pm \arctan\left(\frac{b}{2f'}\right), \tag{4}$$

where f' is the focal length of the first imaging system.

Figure 5 is the schematic diagram for the meridian field. Here, ω_1 is the meridian field angle corresponding to the first step reflecting surface. The first step reflecting surface is placed where a zero OPD is generated. ω_1 is given by

$$\omega_1 \in \left[\arctan\left[\frac{(-0.5N)a}{f'}\right], \arctan\left[\frac{(-0.5N+1)a}{f'+d}\right]\right], \tag{5}$$

where N is the total number of steps and d is the height of each step. The meridian field angle ω_n for the nth-step reflecting surface is

$$\omega_n \in \left[\arctan\left[\frac{(-0.5N+n-1)a}{f'+(n-1)d}\right], \arctan\left[\frac{(-0.5N+n)a}{f'+nd}\right]\right]. \tag{6}$$

The OPD is the same in the field angle domain $W \times \omega_n$. The relationship between the OPDs and the field angles is shown in Fig. 6.

In this IFIS, the edges of the micro-mirrors can be imaged on the MWIR detector to form vertical patterns. That could make it difficult to observe the interference fringes. Fortunately, these vertical patterns can be

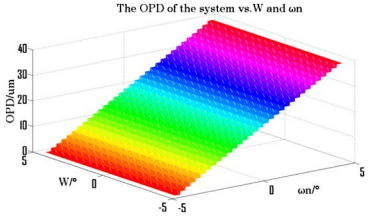

Fig. 6. Schematic diagram of the OPD of the system as a function of W and ω_n.

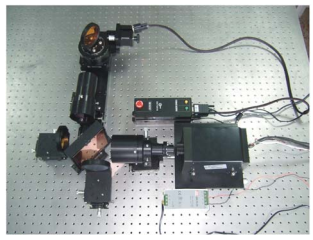

Fig. 7. Photo of the breadboard of this setup.

removed by a method of data processing, so they will not disturb the intensity of the interference image.

The setup was built and experiments have been done to test a target "FTIS" in a laboratory. In this system, the step number is $N = 32$ and the height is $d = 0.625$ μm. Thus, from Eq. (1), we can get that the maximum OPD is $\delta_{\max} = 40$ μm. Thus, the spectrum resolution of this system is equal to $\lambda^2/\delta_{\max}$, which is about 0.4 μm for the wavelength of 4 μm. In this experimental setup, the camera is a cooled HgCdTe detector array of 320 × 256 pixels. Its f-number is 4 and the spectral band is 3.7–4.8 μm. The size of a single pixel is 30 μm. The first imaging system uses a lens with a focal length of 200 mm. The imaging numerical aperture is 0.0308 and the field of view is ±4.6°. The second imaging system uses two lens groups to complete the imaging and interference process. Its object height is 22.5 mm and the magnification is 0.24. The spectral band of the coating in the above optical components is 3.7–4.8 μm. The photo of the breadboard of this setup is shown in Fig. 7.

In this experiment, an infrared lamp was used to illuminate the target. As a result, a polychromatic light interferogram was obtained. The results are shown in Fig. 8 for (a) the image of the multi-step micro- mirrors; (b) the image of the target on the multi-step micro-mirrors; (c) the image of the target on the plane mirror; and (d) the interference image of the target object. As mentioned above, the OPDs increase from 0 to 40 μm as the number of steps increases from 0 to 32. The effects of different OPDs can be seen in Fig. 8(d) whose left side has the most significant interference with zero OPD. As the number of steps increases, the interference weakens. On the right side of Fig. 8(d) where the OPD reaches a maximum, it is difficult to observe any interference.

To further verify the interference pattern, the lower part of the plane mirror was covered. The result is given in Fig. 9 where (a) is the original interference pattern without covering, and (b) shows no interference at the lower part because of covering. From Fig. 9, we could also see the coincidence between the widths of the

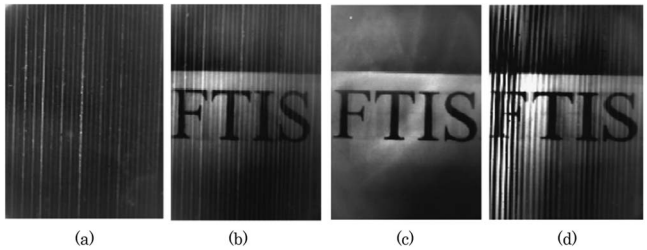

Fig. 8. Laboratory experimental results for the imaging spectrometer.

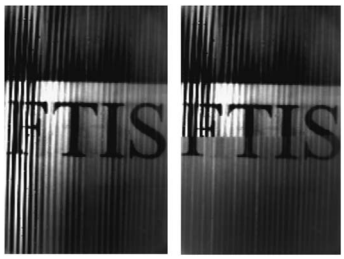

(a) (b)

Fig. 9. Verification of the interference pattern for the imaging spectrometer.

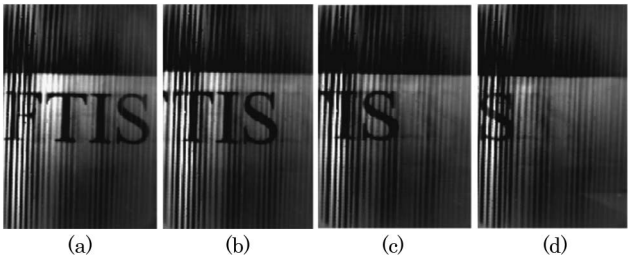

(a) (b) (c) (d)

Fig. 10. Interference images of the object target at four different moments.

interference fringes and the reflecting surface of the multi-step micro-mirrors. The above two points verify that the interference is generated by the OPDs between the plane mirror and the multi-step micro-mirrors.

By rotating the scanning mirror, the windowing process was tested. For N-step micro-mirrors, N scanning images of the target were obtained, and four of them are shown in Fig. 10 where the four letters of the target "FTIS" successively go through the zero OPD position. In the scanning process, only the image of the target object has moved; the position of the interference does not change. This demonstrates that the proposed imaging spectrometer works and the experimental results are consistent with the theoretical analysis.

In summary, a novel spatio-temporally modulated infrared IFTS is proposed. In this design, it adopts multi-step micro-mirrors to replace the moving mirror. This results in the advantages of a stable and static structure. The system has no slit, so it has an advantage of a large luminous flux. Such advantages are expected to benefit a variety of applications. However, this current setup has a relatively low spectral resolution because of the low number of steps of the multi-step micro-mirrors. Future work on this imaging system will include adding steps to the multi-step micro-mirrors to improve spectral resolution, as well as field experiments.

The authors gratefully acknowledge Prof. Ding Yi Wang of Xi'an Jiaotong University for his help and Dr. Cong Feng for many helpful discussions. The research described in this Letter was funded by the National Natural Science Foundation of China (Grant Nos. 61376122, 61027010, 60977062, 61007023), Science and Technology Development Plan of Jilin Province (Grant Nos. 20130206010GX, 201205025), Changchun Science Development Plan (Grant Nos. 2013261, 2011131), and State Key Laboratory of Applied Optics Independent Fund.

References

1. Y. Fereec, J. Taboury, H. Sauer, P. Chavel, P. Fournet, C. Coudarin, J. Deschams, and J. Primot, Appl. Opt. **50**, 5894 (2011).
2. S. A. Rinehart, D. T. Leisawitz, M. R. Bolcar, K. M. Chaprnka, R. G. Lyon, S. F. Maher, N. Memarsadeghi, E. J. Sinukoff, and E. Teichman, Proc. SPIE **7734**, 773421 (2010).
3. J. R. Dupuis and M. S. Ünlü, Opt. Lett. **33**, 1368 (2008).
4. M. Pisani and M. Zucco, Opt. Express **17**, 8319 (2009).
5. J. Li, J. P. Zhu, C. Qi, C. L. Zhen, B. Gao, Y. Y. Zhang, and X. Hou, Opt. Express **21**, 10182 (2013).
6. Q. L. Li, X. F. He, Y. T. Wang, H. Y. Liu, D. R. Xu, and F. M. Guo, J. Biomed. Opt. **18**, 100901 (2013).
7. M. R. Carter, C. L. Bennrtt, D. J. Fields, and F. D. Lee, Proc. SPIE **2480**, 380 (1995).
8. T. Inoue, K. Itoh, and Y. Ichioka, Opt. Lett. **16**, 934 (1991).
9. L. J. Otten, R. G. Sellar, and J. B. Rafert, Proc. SPIE. **2583**, 566 (1995).
10. T. K. Mu, C. M. Zhang, W. Y. Ren, and C. L. Jia, Opt. Lett. **37**, 3507 (2012).
11. P. L. Hanst, Appl. Opt. **17**, 1360 (1978).
12. C. S.-C. Yang, E. E. Brown, U. Hommerich, F. Jin, S. B. Trivedi, A. C. Samuels, and A. P. Snyder, Appl. Spectrosc. **66**, 1397 (2012).
13. C. M. Snively, S. Katzenberger, G. Oskarsdottir, and J. Lauterbach, Opt. Lett. **24**, 1841 (1999).
14. F. Adler, P. Maslowski, A. Foltynowicz, K. C. Cossel, T. C. Briles, I. Hartl, and J. Ye, Opt. Express **18**, 21861 (2010).
15. K. D. Möller, Appl. Opt. **34**, 1493 (1995).
16. A. Rosak and F. Tintó, *The 5th International Conference on Space Optics* (2004), pp. 67–71.
17. E. Ivanov, J. Opt. A Pure Appl. Opt. **2**, 519 (2000).
18. X. H. Jian, C. M. Zhang, L. Zhang, and B. C. Zhao, Opt. Express **18**, 5674 (2010).
19. C. M. Zhang and X. H. Jian, Opt. Lett. **35**, 366 (2010).
20. A. Hirai, T. Inoue, K. Itoh, and Y. Ichioka, Opt. Rev. **1**, 205 (1994).
21. P. G. Lucey, M. Wood, and S. T. Crites, Proc. SPIE **8390** 839003 (2012).
22. M. Born and E. Wolf, *Principles of Optics* (Publishing House of Electronics Industry, 2009).